

# Printed Degradable Optical Waveguides for Guiding Light into Tissue

Jun Feng, Yijun Zheng, Shardul Bhusari, Maria Villiou, Samuel Pearson, and Aránzazu del Campo\*

Optogenetics and photonic technologies are changing the future of medicine. To implement light-based therapies in the clinic, patient-friendly devices that can deliver light inside the body while offering tunable properties and compatibility with soft tissues are needed. Here extrusion printing of degradable, hydrogel-based optical waveguides with optical losses as low as  $0.1 \text{ dB cm}^{-1}$  at visible wavelengths is described. Core-only and core-cladding fibers are printed at room temperature from polyethylene glycol (PEG)-based and PEG/Pluronic precursors, and cured by in situ photopolymerization. The obtained waveguides are flexible, with mechanical properties tunable within a tissue-compatible range. Degradation times are also tunable by adjusting the molar mass of the diacrylate gel precursors, which are synthesized by linking PEG diacrylate (PEGDA) with varying proportions of DL-dithiothreitol (DTT). The printed waveguides are used to activate photochemical and optogenetic processes in close-to-physiological environments. Light-triggered migration of cells in a photoresponsive 3D hydrogel and drug release from an optogenetically-engineered living material by delivering light across  $>5 \text{ cm}$  of muscle tissue are demonstrated. These results quantify the in vitro performance, and reflect the potential of the printed degradable fibers for in vivo and clinical applications.

## 1. Introduction

Optogenetics and the development of optical technologies for medical interventions are revolutionizing therapy.<sup>[1]</sup> The

J. Feng, Dr. Y. Zheng,<sup>[†]</sup> S. Bhusari, M. Villiou, Dr. S. Pearson, Prof. A. del Campo  
INM–Leibniz Institute for New Materials  
Campus D2 2, Saarbrücken 66123, Germany  
E-mail: Aranzazu.DelCampo@leibniz-inm.de

J. Feng, S. Bhusari, M. Villiou, Prof. A. del Campo  
Chemistry Department  
Saarland University  
Saarbrücken 66123, Germany

 The ORCID identification number(s) for the author(s) of this article can be found under <https://doi.org/10.1002/adfm.202004327>.

<sup>[†]</sup>Present address: School of Physical Science and Technology, ShanghaiTech University, Shanghai 201210, China

© 2020 The Authors. Published by Wiley-VCH GmbH. This is an open access article under the terms of the Creative Commons Attribution-NonCommercial License, which permits use, distribution and reproduction in any medium, provided the original work is properly cited and is not used for commercial purposes.

DOI: 10.1002/adfm.202004327

temporal and spatial control offered by light-sensitive processes, and the possibility to regulate therapeutic dose by light intensity<sup>[2]</sup> are inherent advantages of using light for modulating biological processes.<sup>[3]</sup> To implement light-based therapies in the clinic, light has to be delivered inside the body. However, absorption and scattering by tissues limit light penetration depth to just a few millimeters in the near-infrared region, and even less at shorter wavelengths.<sup>[1d,4]</sup> Overcoming the limited penetration depth of light in tissue is therefore a challenge for photo-based therapies.<sup>[4]</sup> Implantable optical fibers and light-emitting diodes (LEDs) have been used to efficiently bring light to in vivo targets.<sup>[5]</sup> However, these devices are typically made from stiff materials and are not always appropriate for implantation in soft tissues. Moreover, for short-term applications, the devices have to be removed from the body in a second operation.<sup>[6]</sup> More compliant biomaterials that exhibit biodegradability could offer significant advantages for appli-

cations requiring short-term light delivery, as recently shown in photochemical tissue bonding for wound closure<sup>[4]</sup> and temporary optogenetic neuron stimulation.<sup>[7]</sup> Light-regulated processes in living organisms are also specifically designed to be activated at low irradiation doses, while optical waveguides and LEDs currently in use for optogenetics and medical photonics are derived from devices in electronics or communication technologies and, in most cases, are over-engineered for biomedical applications. Simpler devices in terms of composition and design could offer the required optical performance while better meeting the biocompatibility requirements for clinical implementation.

Soft polymeric biomaterials have been used as alternatives to silica for fabricating optical waveguides, and may be better suited to medical scenarios. Waveguides made from natural polymers such as silkworm<sup>[8]</sup> and spider<sup>[9]</sup> silk, cellulose,<sup>[10]</sup> agarose,<sup>[11]</sup> and gelatin<sup>[12]</sup> have been reported, offering biocompatibility and degradability. In order to facilitate standardizable physical/chemical/biological properties,<sup>[13]</sup> degradable and non-degradable synthetic polymers have also been explored for optical waveguides. Polyethylene glycol diacrylate (PEGDA)-based hydrogels,<sup>[14]</sup> polyacrylamide (PAM)-based hydrogels,<sup>[15]</sup> polydimethylsiloxane,<sup>[16]</sup> poly(lactic acid),<sup>[4,7,17]</sup> poly(lactic-co-glycolic acid),<sup>[4]</sup> polydioxanone,<sup>[18]</sup> polyethersulfone,<sup>[19]</sup> and citrate-based biomaterials<sup>[20]</sup>

have all been reported. The waveguiding performance of these materials is far lower than optical waveguides from silica or polymers used in technical applications. For example, attenuation values as low as 0.2 dB km<sup>-1</sup> at 1550 nm can be achieved in silica optical fibers,<sup>[21]</sup> while polymeric optical fibers reach only 0.01 dB cm<sup>-1</sup> at 840 nm.<sup>[22]</sup> The attenuation values in reported biomaterial-based optical waveguides range from 0.1 to 28 dB cm<sup>-1</sup>.<sup>[6]</sup> Materials showing attenuation values between 0.17 and 1.64 dB cm<sup>-1</sup><sup>[7,14a,d]</sup> have proven sufficient as waveguides for activating processes in vivo using wavelengths in the 450 to 640 nm range. In order to improve light guiding properties, core-cladding fiber designs have been developed to encourage total internal reflection and reduce light loss. For example, alginate has been employed as a cladding material for PEGDA or PAM cores, and the fabricated core/cladding waveguides exhibited 20–60% less optical loss than single fibers.<sup>[14d,g,15a]</sup>

Biomaterial-based optical waveguides are typically fabricated by curing pre-polymer solutions in a mold,<sup>[8b,14d,g,i,k-m,15a,16d-g,20]</sup> with cladding introduced in a subsequent dip-coating and curing process. This is a multistep batch process which is difficult to scale up, does not easily allow changes in fiber geometry, and is not well suited to miniaturized or multimaterial devices. We envisage printing as a promising technological alternative, which may allow single<sup>[8a]</sup> (or core-shell<sup>[23]</sup>) fibers of soft functional materials to be deposited in the desired geometry in one step by (coaxial) extrusion. However, only one printed optical waveguide has been reported to date, in which a single fiber of silk fibroin was produced by printing into a coagulation bath.<sup>[8a]</sup> Printable materials with adequate optical properties for waveguiding need to be identified. In this article, we describe a degradable PEG-based printable ink composition<sup>[24]</sup> and a printing method for fabricating single and core/cladding optical waveguides by coaxial printing.

Among biomaterials used for optical waveguides, PEGDA-based hydrogels present a good balance between transparency and biocompatibility in terms of non-immunogenicity and resistance to protein adsorption.<sup>[6]</sup> However, waveguiding is more effective if there is a large refractive index (RI) difference between the waveguide and surroundings/cladding. The RI of a hydrogel increases linearly with the polymer content, therefore higher concentrations of polymer are preferred in hydrogel waveguides. Low molar mass PEGDA (e.g., 500 or 700 Da) has been shown to form transparent hydrogels above 50% w/v,<sup>[14a,d]</sup> but the stiffness of these gels is relatively high (22 MPa with 65% v/v of 508 Da PEGDA<sup>[25]</sup>). Higher molar mass PEGDA (e.g., >2 kDa) forms transparent (and less stiff) hydrogels at all concentrations,<sup>[6,14a,d]</sup> but producing high concentration solutions requires long dissolution times (many hours) or can even be unattainable. Obtaining soft, easy-to-handle, high concentration PEG-based hydrogels would require modification to the PEG backbone to render it less prone to crystallization and therefore improve solubility. Furthermore, PEGDA units contain only two degradable groups per chain (between each vinyl group and the PEG backbone), and these ester groups exhibit slow hydrolysis. Introducing more hydrolytically labile linkages into PEG-based hydrogels is attractive for applications requiring faster degradation.

Here we present printable DL-dithiothreitol (DTT)-bridged PEGDA (PEGDA-DTT)<sup>[24]</sup> as a suitable PEG-based hydrogel precursor for manufacturing optical waveguides. The thioether linkages distributed in the backbone of these precursors extend the polymer chains and provide OH side groups which inhibit

precursor crystallinity, rendering all the precursors liquid, and rapidly soluble in water. Furthermore, the linkages make the ester bonds less hydrolytically stable than those in PEGDA, meaning that faster degradability can be achieved as shown by Hudalla.<sup>[24]</sup> Adjusting the molar mass of the PEGDA-DTT allows tuning of mechanical properties (Young's modulus 100 kPa–8 MPa) and degradation rates (1 to several months). We present printable formulations of PEGDA-DTT with sufficient light guiding performance in air (0.1–0.4 dB cm<sup>-1</sup>) and in tissue (0.25–0.7 dB cm<sup>-1</sup>) for activating biological processes. Two proof-of-concept examples demonstrate the performance of the printed waveguides by stimulating photochemical processes at wavelengths 405 and 450 nm across non-transparent muscle tissues. Core/cladding designs with improved optical properties by coaxial printing with medically-approved Pluronic F127 as cladding material are also described.

## 2. Results and Discussion

### 2.1. Synthesis of PEGDA-DTT Pre-Polymers

In order to incorporate tunable degradation properties into the PEG-waveguides, acrylate groups of PEGDA were reacted with thiol groups of DTT to afford PEGDA-DTT precursors by Michael-type addition reaction in water in the presence of triethylamine (Figure 1A).<sup>[24]</sup> An excess of PEGDA was used in order to obtain acrylate-terminated PEGDA-DTT chains for later crosslinking and hydrogel formation. The kinetics of the reaction were followed by monitoring the free thiol groups in the mixture using a fluorometric thiol assay. The thiol concentration decreases by more than 5 orders of magnitude within the first minute (Figure 1B), and decreases further in 10 min. The reaction is almost quantitative, with the final thiol concentration below 1 μM. The consumption of acrylate groups originating from PEGDA was quantified by <sup>1</sup>H NMR spectroscopy for each DTT/PEGDA ratio (Figure S1, Supporting Information). The measured concentration of remaining acrylate groups, which reside at the termini of the resulting PEGDA-DTT chains, decreased with increasing feed ratio of DTT to PEGDA and was consistent with the expected theoretical estimation (Table 1). PEGDA-DTT products were named according to the feed ratio of DTT to PEGDA used for synthesis, that is, PEGDA-DTT-50, PEGDA-DTT-75, PEGDA-DTT-875, and PEGDA-DTT-93.75 for ratios 0.5, 0.75, 0.875, and 0.9375 between DTT and PEGDA. The freeze dried PEGDA-DTT products were viscous liquids at room temperature, and dissolved rapidly in water (unlike comparable molar mass PEGDA). Their viscosity increased with the feed ratio of DTT to PEGDA (Figure 1C and Table 1) as a consequence of the increasing chain length. The higher molar masses of the PEGDA-DTT products with increasing content of DTT bridges was confirmed by size exclusion chromatography (SEC) analysis (Table 1). The dispersities are in the range of 1.8–2.8, and increase with increasing DTT/PEGDA ratio (Table 1).

### 2.2. Synthesis and Physicochemical Properties of PEGDA-DTT Hydrogels

PEGDA-DTT hydrogels were prepared by photocrosslinking water solutions of PEGDA-DTT precursors at different

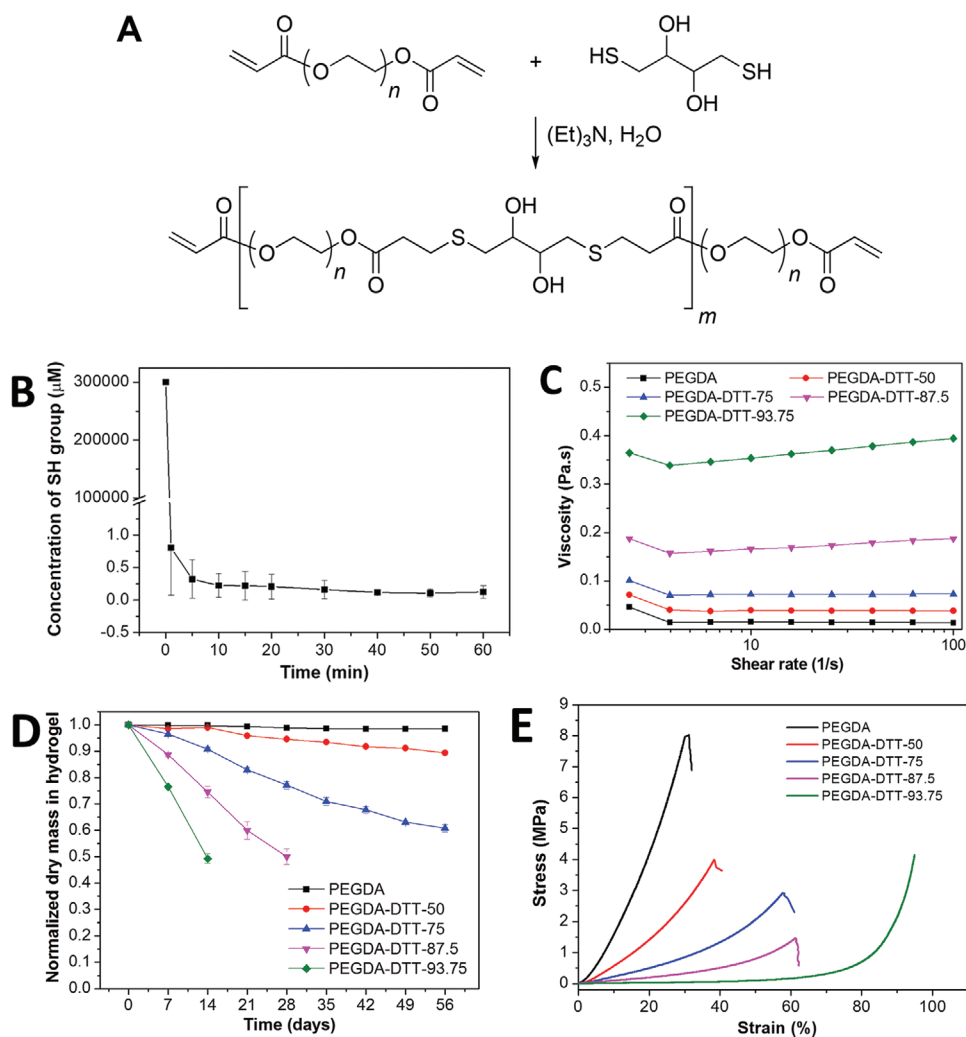


**Figure 1.** Chemical design and physical properties of PEGDA-DTT pre-polymers and hydrogels. A) Synthesis of PEGDA-DTT polymer from PEGDA and DTT precursors. B) Kinetics of the Michael addition reaction between acrylate groups of PEGDA and thiol groups of DTT as followed by a fluorometric thiol assay kit. C) The viscosity of PEGDA-DTT solutions (50 wt%) measured at increasing shear rate at room temperature; D) Degradation kinetic curves of 70 wt% PEGDA-DTT hydrogels. The graph shows the normalized dry mass of the gel as function of incubation time in PBS at 37 °C. E) Stress–strain curves from compressive tests of 70 wt% PEGDA-DTT hydrogels.

concentrations using Irgacure 2959 as initiator and a 365 nm light source. Each polymer solution was polymerized within a Teflon ring of diameter 5 mm and thickness 3 mm that was sandwiched between two glass slides. Gels were homogeneous and transparent, and became less stiff and pale yellow with increasing DTT/PEGDA ratio. The swelling ratio, degradation rate, and Young's modulus of the PEG-DTT hydrogels were characterized as a function of DTT/PEGDA ratio. The swelling ratio increased from 73% to 539% with increasing DTT/PEGDA ratio (Table 1). This is in agreement with a lower crosslinking degree expected from the lower number of acrylate groups per unit mass, which generates a larger mesh size and therefore a higher water uptake. The degradation kinetics of the hydrogels were measured in PBS at 37 °C over 56 days. Across the four compositions, the degradation rate increased with increasing pre-polymer chain length (Figure 1D), that is, with increasing number of DTT units per pre-polymer chain.

The proximal thioether bonds provide a more positive partial charge to the carbonyl carbons of the acrylate esters, forming the expected degradation sites of the hydrogels by facilitating reaction with nucleophilic hydroxide anions as the primary step of base-catalyzed ester hydrolysis.<sup>[24,26]</sup> Over the same timescale, PEGDA 700 Da hydrogel did not degrade (Figure 1D). These experiments demonstrate that PEGDA-DTT gels allow modulation of the degradation kinetics by simply varying the feed ratio of DTT to PEGDA.

The mechanical properties of PEGDA-DTT hydrogels were analyzed with compression tests. Figure 1E shows the corresponding stress-strain curves. The Young's modulus of 70 wt% hydrogels decreased from 22 MPa to 140 kPa with increasing DTT/PEGDA ratio from 0 to 0.9375 (Table 1). The decreasing stiffness is attributed to the decreasing crosslinking degree as the length of the PEGDA-DTT precursors increase. The stress at break decreased from 7.7 MPa

**Table 1.** Physicochemical properties of PEGDA-DTT pre-polymers and hydrogels.

	PEGDA-700	PEGDA-DTT-50	PEGDA-DTT-75	PEGDA-DTT-87.5	PEGDA-DTT-93.75
Relative content of acrylate groups (calculated) [%]	100	50	25	12.5	6.25
Relative content of acrylate groups (measured) [%] <sup>a)</sup>	100	49.4 ± 0.6	24.4 ± 1.6	12.2 ± 1.0	6.4 ± 0.1
Viscosity [Pa s] <sup>b)</sup>	0.046	0.071	0.101	0.187	0.365
$M_n$ [Da] <sup>c)</sup>	700	4272	6134	9052	11 879
Dispersity <sup>c)</sup>	–	1.81	2.06	2.56	2.83
Swelling ratio in water [%] <sup>d)</sup>	73 ± 2	108 ± 2	186 ± 2	291 ± 1	539 ± 23
Swelling ratio in tissue [%] <sup>d)</sup>	16 ± 2	17 ± 1	44 ± 1	87 ± 2	/
Young's modulus [MPa] <sup>e)</sup>	22.8 ± 1.5	7.9 ± 0.2	2.7 ± 0.3	0.9 ± 0.1	0.14 ± 0.02
Stress at break [MPa] <sup>e)</sup>	7.6 ± 0.9	3.9 ± 0.5	2.9 ± 0.8	1.8 ± 0.6	no break
Strain at break [%] <sup>e)</sup>	32 ± 3	38 ± 3	54 ± 4	65 ± 3	no break

<sup>a)</sup>The percentage of initial acrylate groups remaining unreacted in PEGDA-DTT products was measured by <sup>1</sup>H NMR spectroscopy; <sup>b)</sup>the viscosities of the precursor solutions were measured by flow sweep on a rheometer at polymer concentrations of 50 wt% in water; <sup>c)</sup>the number-averaged molar mass ( $M_n$ ) and dispersity values for PEGDA-DTT products were measured by SEC, while  $M_n$  of PEGDA-700 is from the supplier; <sup>d)</sup>swelling ratios correspond to 70 wt% PEGDA-DTT hydrogels or fibers after immersion in water for 24 h or after being sandwiched between two pieces of muscle tissue for 1 h; <sup>e)</sup>Young's moduli, and stress and strain at break, were obtained from compression tests with 70 wt% PEGDA-DTT hydrogels.

to less than 1.8 MPa and the strain at break increased from 32% to more than 65% with increasing DTT/PEGDA ratio (Table 1). These results indicate that the mechanical properties of PEGDA-DTT hydrogels can be tuned by two orders of magnitude by simply changing the ratio of DTT to PEGDA. This is a relevant feature for the fabrication of optical waveguides to be used for clinical applications as it allows adaptation of the waveguide mechanics to the mechanics of the specific tissue in the application.

### 2.3. Optical Properties of PEGDA-DTT Hydrogels

Absorption and scattering are the most important factors affecting the light guiding properties of materials. For biomaterials, especially polymeric biomaterials, intrinsic optical loss originates from absorption, including electronic and vibrational absorption,<sup>[22]</sup> and scattering due to density fluctuations, compositional inhomogeneities, and large inclusions.<sup>[22]</sup> The most important extrinsic factor for effective lightguiding is the RI of the surrounding medium, which needs to be lower than that of the waveguide in order to achieve total internal reflection. Since the RI of human tissues ranges from 1.38 to 1.51,<sup>[27]</sup> achieving total internal reflection can be a challenge for hydrogel waveguides with high water contents (RI water = 1.33).

The absorption of PEGDA-DTT hydrogels within the spectral range from 350 to 800 nm was measured by UV–vis spectrophotometry (Figure 2A and Figure S2A, Supporting Information). Each PEGDA/DTT composition was analyzed at different polymer concentrations ranging from 10 wt% up to 70 wt% (in 10 wt% increments). Below 400 nm, absorbance was high in all systems due to electronic transitions of the organic groups.<sup>[28]</sup> Above 400 nm, the introduction of DTT significantly lowered the absorbance versus the PEGDA 700 Da reference hydrogel, in particular at polymer concentrations below 50 wt% (Figure S2A, Supporting Information). At low concentrations,

the transparency of PEGDA hydrogels is known to increase with increasing molar mass since phase segregation is avoided.<sup>[6]</sup> The same effect is observed here. PEGDA-DTT also displays pendant OH groups along the polymer chain (contributed by the DTT units, Figure 1A) which could further enhance hydration of the formed polymer networks. Precursor solutions and derived hydrogels with 75 mol% of DTT were transparent at all polymer concentrations (Figure S2A,B, Supporting Information).

The scattering properties of PEGDA-DTT hydrogels were compared using a home-made setup (Scheme S1, Supporting Information). A 520 nm laser passed through a cuvette containing the hydrogel. The scattered light was captured with a camera situated perpendicular to the incident light beam. The polymer chains in hydrogels are generally amorphous, with scattering typically arising from structural inhomogeneities in the polymer network which produce fluctuations in RI.<sup>[6]</sup> Phase segregation, such as that observed in PEGDA 700 Da hydrogels at <50 wt% polymer content, is an example of drastic inhomogeneity which gives rise to extensive scattering and therefore opaque hydrogels. Even transparent hydrogels, however, possess imperfect polymer networks, and scattering due to network inhomogeneity is therefore inevitable. All four PEGDA-DTT hydrogels showed ≈50% less scattering than PEGDA hydrogel at a polymer concentration of 70 wt% (Figure 2B). For a particular PEGDA-DTT composition, gel scattering ratio decreased with polymer concentration; the 80 wt% gel made from PEGDA-DTT-87.5 for example shows less than half the scattering intensity of the 40 wt% gel (Figure S2C, Supporting Information). These data are in agreement with the formation of more homogeneous polymer networks, which reduces scattering, and with the less favored phase separation in PEGDA chains at higher polymer concentrations as reported by other authors.<sup>[6,14a]</sup> The scattering observed at polymer concentrations >50 wt% is mainly associated with Mie-type light scattering of partially disordered networks and is unavoidable.<sup>[6]</sup>

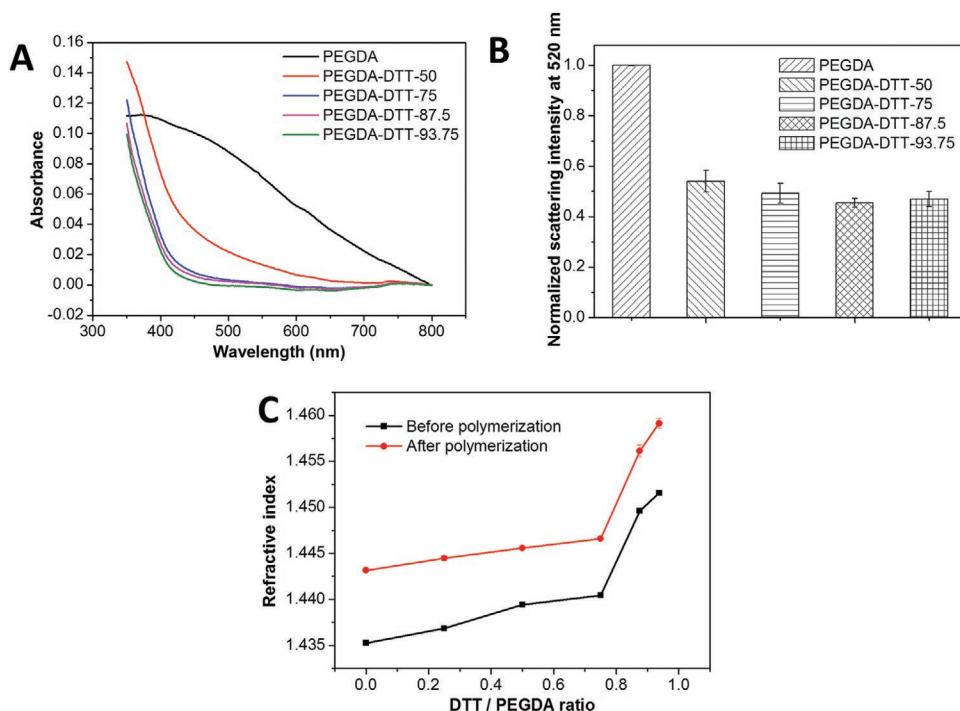


**Figure 2.** Optical properties of PEGDA-DTT hydrogels. A) UV-vis spectra of 10 wt% PEGDA-DTT hydrogels. B) The relative scattering of 70 wt% PEGDA-DTT hydrogels with different DTT/PEGDA ratios; C) the RI of 70 wt% PEGDA-DTT hydrogels before and after polymerization.

The RI of 70 wt% PEGDA-DTT hydrogels increased with DTT content from 1.435 to 1.46 (Figure 2C), and indicates that the introduction of DTT bridges could improve the light confinement ability of PEGDA-DTT waveguides in tissues and lead to optical waveguides with higher optical performance. The RI of PEGDA-DTT also increased with polymer content. Figure S2D, Supporting Information shows that the RI of PEGDA-DTT-93.75 gels increased linearly from 1.36 to 1.46 when the polymer concentration changed from 20 wt% to 70 wt%.

In summary, the introduction of DTT bridges in PEGDA precursor leads to a comprehensive improvement in hydrogel optical properties versus PEGDA alone: PEGDA-DTT-*X* hydrogels with *X* ≥ 75 mol% are highly transparent in the visible wavelength range for all the tested concentrations (5 to 70 wt%), with higher concentrations showing additional benefits of higher RI and lower light scattering. These are all relevant properties for the application of PEGDA-DTT hydrogels as optical waveguides, and suggest that higher concentrations of PEGDA-DTT could be more suitable for producing efficient waveguides.

#### 2.4. In Vitro Cytocompatibility of PEGDA-DTT Hydrogels

The cytocompatibility of the PEGDA-DTT hydrogels was tested in vitro using the live/dead assay with retinal pigmented epithelial (RPE1) cells. Cells were cultured on tissue culture plates and gels were introduced in the cell culture medium. Viabilities of 99% were obtained after 24 and 48 h culture in the presence of all the gels (Figure S3, Supporting Information), demonstrating good cytocompatibility.

#### 2.5. Printing Optical Waveguides

PEGDA-DTT solutions were tested as inks for printing using an extrusion-based printer coupled to an illumination source for in situ photopolymerization (Figure 3A: left and middle). In order to facilitate printing and achieve high shape fidelity of the printed fibers, a transparent silicone tube was inserted at the end of the needle tip (Figure 3A: right).<sup>[23]</sup> The light beam for initiating the radical polymerization of the acrylate groups, leading to crosslinking of the ink, was shone through the silicone tube. Different printing conditions were explored by varying printing pressure between 5 and 55 kPa, illumination intensity between 10–100%, and by using silicone tubes with inner diameter of 310 or 510 μm. The printing of all PEGDA-DTT ink compositions was tested using different concentrations of the polymer precursor and photoinitiator. In general, the printability was higher at higher concentrations of polymer precursor and higher DTT contents. Optimization of the printing conditions generated printability windows for each ink composition, which are detailed in the Supporting Information and summarized in Figure S4, Supporting Information. Within the printability windows, continuous fibers (we tested up to 50 cm length) can be easily printed (Figure 3B). The obtained fibers exhibit high transparency, shape fidelity, and homogeneity, and are flexible. The surface of the printed fibers was smooth as viewed by optical microscopy and scanning electron microscopy (Figure 3B: insets, Figure S5: up, Supporting Information), which is inherited directly from the inner wall of the silicone tube used for curing. The printed fibers become less stiff with increasing DTT content in the ink. Figure 3B shows the higher flexibility of printed PEGDA-DTT-93.75 versus PEGDA-DTT-50

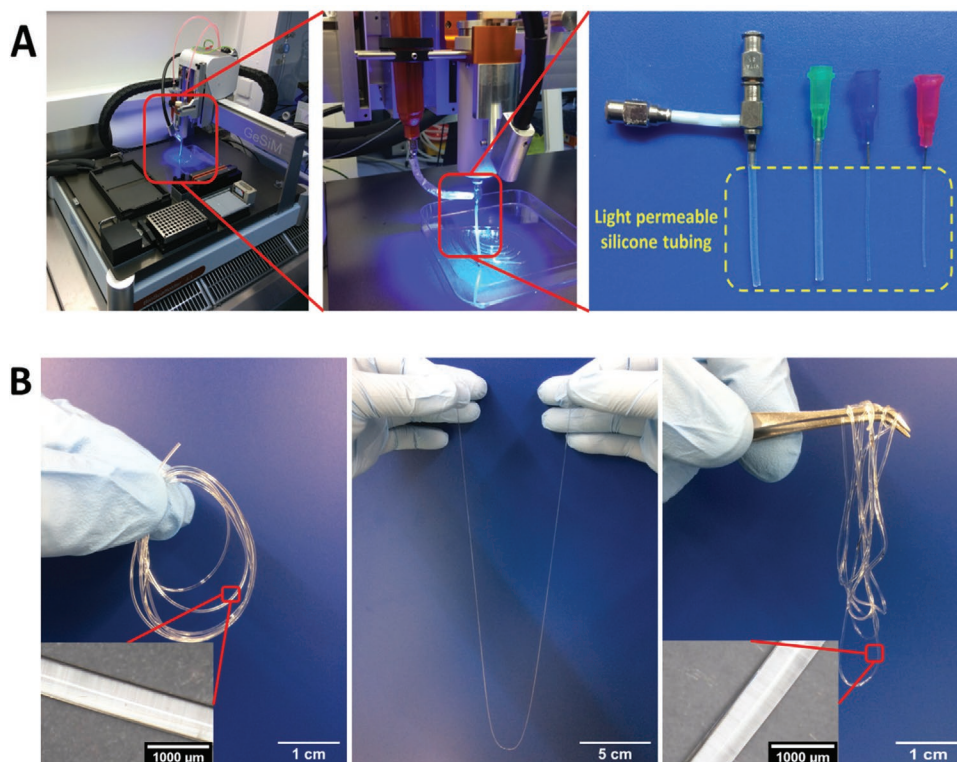


**Figure 3.** A) Printing setup. Left: printing stage of 3D-Bioscaffolder from GESIM; middle: printing head mounted with coaxial needle; right: printing needles extended with silicone tubes. B) Images of 70 wt% PEGDA-DTT fibers printed using the 510  $\mu\text{m}$  silicone tube. Left: PEGDA-DTT-50; middle: PEGDA-DTT-87.5; right: PEGDA-DTT-93.75.

fibers. These results are consistent with the mechanical properties measured on the bulk hydrogels, and demonstrate the possibility to adapt the mechanical properties of the printed fibers to the mechanics of target tissues. However, low stiffness also brings some disadvantages. For example, the more flexible fibers get stuck to themselves more easily and become more difficult to handle (Figure 3B: right).

## 2.6. Optical Properties of the Printed PEGDA-DTT Waveguides

For hydrogel-based optical fibers, obtaining a very smooth surface at the fiber tip is challenging. As shown in Figure S5, Supporting Information, different fibers (with different DTT/PEGDA ratios) demonstrate different roughness at the terminal cross-sections, which affects the efficiency of light in- and out-coupling. To ensure that variable roughness at the fiber ends would not affect our quantification of optical properties, we developed a new method to quantify the light guiding properties of the printed fibers (Scheme S2, Supporting Information) by adapting optical loss measurement protocols from previous reports.<sup>[29]</sup> In a home-made setup, a laser beam (with wavelength 405, 450, or 520 nm) was focused through a plano-convex lens into the proximal end of the printed waveguide. The light propagated along the fiber (Figure S6A,B, Supporting Information), and generated autofluorescence in the material (Figure S6C,D, Supporting Information). Autofluorescence is a reported but underexploited phenomenon in hydrogels devoid

of a traditional fluorophore. A recent study<sup>[30]</sup> established that autofluorescence is apparently universal in carbonyl-containing hydrogels (but is not present in the precursor solutions), with fluorescence lifetime around 1 ns similar to conventional chromophores, and quenching produced by certain metal ions. Autofluorescence intensity is influenced by water content and gel structure, but the underlying mechanism is unknown. Although it has been reported as an inconvenience to be overcome in fluorimetric assays,<sup>[31]</sup> the potential benefits of hydrogel autofluorescence have more recently been explored for label-free tracking of hydrogel formation<sup>[30]</sup> and degradation.<sup>[32]</sup> In this work, we exploit autofluorescence in our fibers to quantify their optical loss independent of the in- and out-coupled light intensity.

A camera was set perpendicular to the fiber axis to take pictures of the autofluorescence. In order to exclude scattered incident light, a 550 nm long-pass filter was applied between camera and fiber, which only allowed the autofluorescence light to pass through. By detecting the attenuation of autofluorescence along the fiber (Figure S6C,D, Supporting Information), the optical losses could be determined. For quantification, the captured images were analyzed by ImageJ software to obtain the autofluorescence intensity at different positions (distance:  $Z$ , intensity:  $I_0$  and  $I_z$ ). The optical loss  $\alpha(\lambda)$  (in dB per length unit) was calculated by Equation (1).<sup>[33]</sup>

$$\alpha(\lambda) = \frac{10}{Z} \log \frac{I_0}{I_z} \quad (1)$$

With this method, the effect of coupling losses on optical losses in fibers can be effectively avoided. No matter how much light is coupled into the fiber, the attenuation of autofluorescence along the fiber is unchanged. Therefore, more accurate optical losses in the fibers can be expected versus the traditional cut-back method, which measures the light intensity emerging from the distal tip of a fiber after it is cut shorter and shorter, and therefore requires accurate values for in-coupled light intensity and out-coupling efficiency in order to accurately determine optical loss.

Printed 70 wt% PEGDA-DTT waveguides show optical losses in air between  $0.1 \text{ dB cm}^{-1}$  (at 520 nm) and  $0.4 \text{ dB cm}^{-1}$  (at 405 nm) (Figure 4A), with higher optical loss at shorter wavelengths mostly a consequence of higher absorbance. The optical loss decreased with increasing polymer concentration (Figure 4B). Two main factors contribute to this trend: i) the higher RI of hydrogels with higher polymer concentration, which facilitates total internal reflection and allows better confinement of light in the waveguide, and ii) hydrogels with higher polymer concentration presented lower scattering. The optical loss was not significantly influenced by the DTT/PEGDA ratio (Figure 4A). The propagation of wavelengths  $\geq 670 \text{ nm}$  was checked visually (Figure S6A,B, Supporting Information). All printed waveguides guided light with wavelength  $\geq 670 \text{ nm}$  to distances greater than 20 cm.

We also characterized the light guiding properties of the printed waveguides through tissue, in order to mimic the real application conditions in a medical scenario. For this purpose, the printed waveguide was sandwiched between two pieces of porcine muscle tissue. The autofluorescence intensity of the waveguide before and after passing through tissue was quantified (Figure S6E, Supporting Information). The optical loss in tissue was higher than in air (Figure 4C). This can be attributed to i) the higher RI of tissue, which narrows the incident angle for total internal reflection, ii) the rough surface of porcine tissue that can cause more scattering than air, and iii) waveguides within tissue uptaking moisture and swelling, which decreases the polymer concentration (Table 1) and the RI to the detriment of light guidance. When sandwiched between porcine muscles, printed fibers with higher DTT contents exhibited a slightly higher optical loss, which can be attributed to the decreasing stiffness (Table 1). The lower stiffness of the fiber favors macro or micro bending when in contact with the tissue, which decreases the light guiding performance of the fiber. Most reported biomaterials-based optical waveguides exhibit optical losses in the range of  $0.1\text{--}28 \text{ dB cm}^{-1}$ .<sup>[6]</sup> The optical waveguides presented in this report, with the additional benefits of tunable mechanics and degradability, are excellent competitors and show optical attenuation values at the low end of this range.

In order to describe the light guiding properties of the waveguides more intuitively, the optical loss values were converted to tissue penetration depths—defined as the distance at which the intensity of autofluorescence decreases to  $1/e$ . The penetration depth increased at longer wavelengths and was 6, 10, and 10 cm for wavelengths of 405, 450, and 520 nm respectively (Figure 4D,E). The penetration depth decreased slightly with higher content of DTT bridges due to the lower stiffness as explained above.

## 2.7. Remote Photoactivation of Biological Processes In Vitro with Printed PEGDA-DTT Fibers

The capability of PEGDA-DTT waveguides to guide light and remotely photoactivate biological processes was tested in vitro. A waveguide was used to deliver 405 or 450 nm light through  $>5 \text{ cm}$  porcine tissue to test two different scenarios (Scheme 1): i) from a tissue regeneration perspective, the possibility to remotely trigger migration of cells from spheroids to colonize a surrounding photoactivatable hydrogel,<sup>[34]</sup> and ii) from a therapeutic perspective, the ability to remotely induce the secretion of a drug from optogenetically-engineered bacteria encapsulated in a hydrogel.<sup>[35]</sup>

### 2.7.1. Application of Printed Optical Fiber to Remotely Control Cell Migration in a Hydrogel

We first tested whether the degradable PEGDA-DTT waveguides could be used to remotely trigger adhesion and migration of cells encapsulated in a photoactivatable hydrogel by generating a cell adhesive ligand only upon light exposure.<sup>[34,36]</sup> For this purpose, L929 fibroblast spheroids were encapsulated in a dextran hydrogel functionalized with the photoactivatable cell adhesive peptide cyclo[RGD(DMNPB)fC] (Figure S7, Supporting Information). The DMNPB group attached to the aspartic acid inhibits the affinity of cyclo(RGDfC) peptide for integrins, while its removal upon light exposure restores the affinity. This peptide has been used for light-mediated control of angiogenesis and inflammation processes in vitro and in vivo.<sup>[34b,36a,37]</sup> Printed PEGDA and PEGDA-DTT waveguides of 7 cm length were used to guide light to irradiate the cell-hydrogel construct across 5 cm of porcine muscle (Scheme 1). A laser (405 nm, 4.5 mW) was focused on the proximal end of the fiber, and the light intensity at the distal end was measured to be in the range of  $5\text{--}50 \text{ mW cm}^{-2}$  (Table S1, Supporting Information). This intensity was expected to be sufficient to activate the photocleavage of DMNPB. The footprint of the out-coupled light on the dextran hydrogel was in the range of  $1\text{--}4 \text{ mm}^2$ , which is much larger than the diameter of fibroblast spheroids. Spheroids encapsulated in the irradiated volume were therefore completely surrounded by uncaged RGD ligands, and constituent cells were expected to migrate isotropically. After irradiation (15 min), the hydrogels were cultured for a further 2 days and imaged by confocal microscopy. Encapsulated fibroblasts migrated out of the spheroid into the surrounding region (Figure 5C–F) in irradiated cyclo([RGD(DMNPB)fC]) functionalized hydrogels, but they remained confined in the spheroids in the absence of light (Figure 5B) or in irradiated gels that had not been modified with the adhesive peptide (Figure 5A). These results demonstrate that the light doses delivered by all four waveguide compositions were sufficient to trigger DMNPB photocleavage across 5 cm of tissue. Despite the irradiance values differing in the range  $5\text{--}50 \text{ mW cm}^{-2}$  (Table S1, Supporting Information) across the four fiber compositions, the 15 min exposure time was expected to be sufficient for essentially complete photocleavage of the DMNPB groups in all cases, and explains why cell migration is qualitatively similar in Figure 5C–F. The possibility to remotely control cell behavior in

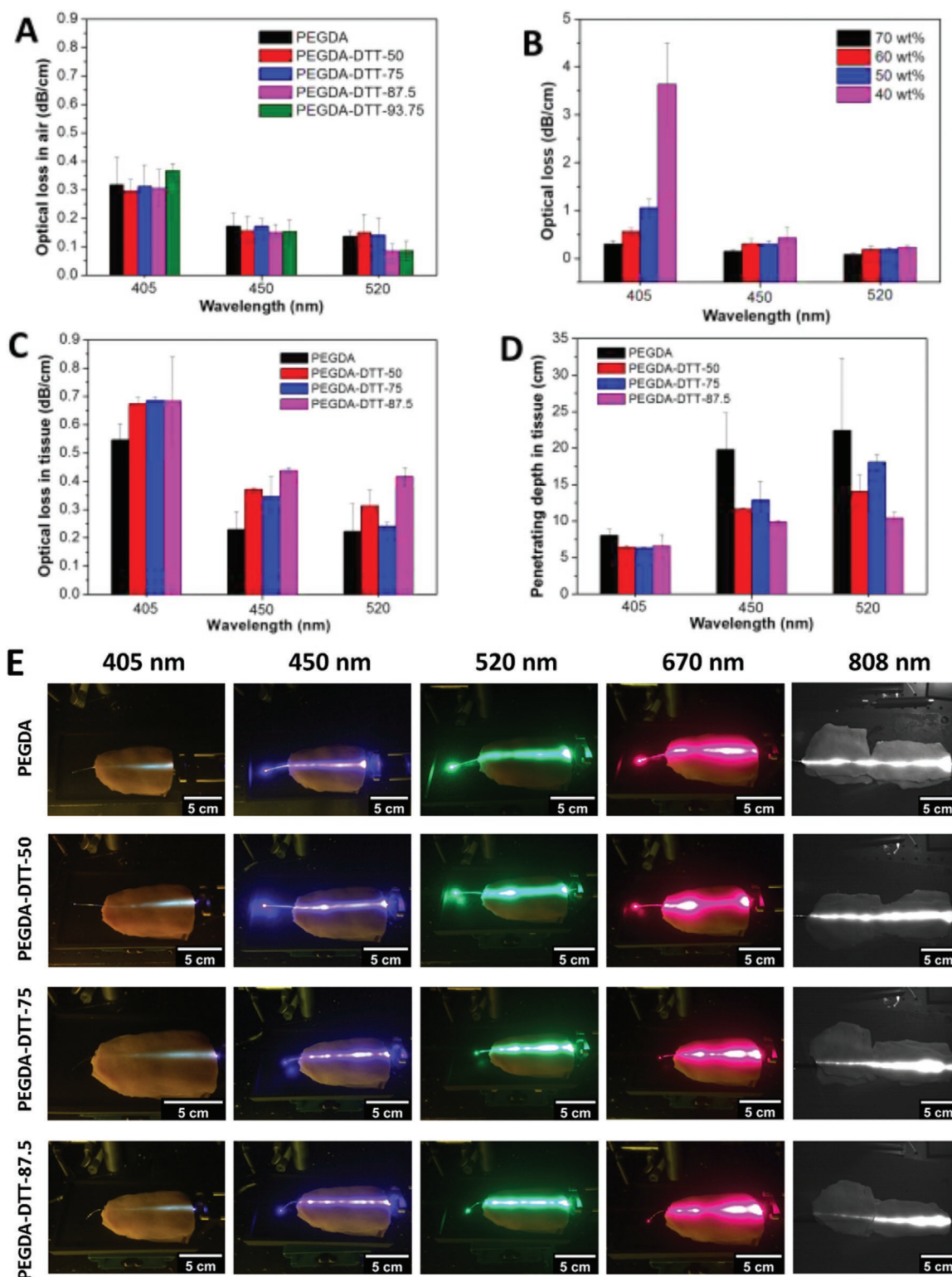
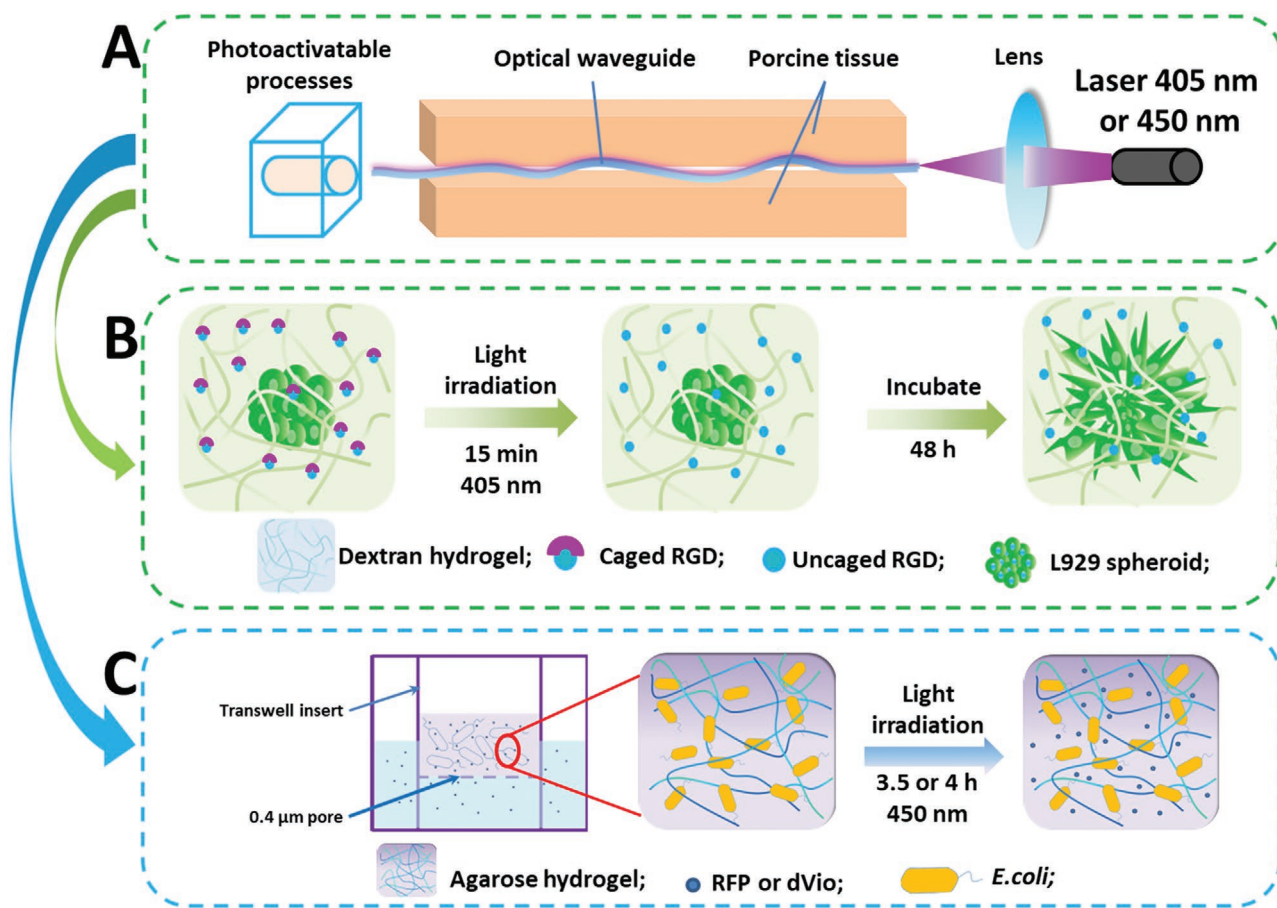


**Figure 4.** Waveguiding properties of PEGDA-DTT printed fibers. A) Optical loss in air measured at different wavelengths in printed 70 wt% PEGDA-DTT waveguides with increasing DTT concentration. B) Optical loss in air measured at different wavelengths in printed PEGDA-DTT-87.5 waveguides with increasing polymer concentration (40–70 wt%). C) Optical loss in tissue measured at different wavelengths in printed 70 wt% PEGDA-DTT waveguides with increasing DTT concentration. D) Tissue penetration depth of guided light by printed 70 wt% PEGDA-DTT waveguides with increasing DTT concentration. E) Images of waveguides sandwiched in tissue and coupled to lasers of different wavelengths. All experiments were repeated at least three times.



**Scheme 1.** Proof-of-principle scenarios for the application of PEGDA-DTT optical waveguides. A) Setup used to deliver light to a targeted destination by waveguides through tissue. B) 3D culture of a fibroblast spheroid within a polymeric matrix modified with photoactivatable cell adhesive ligands. After light exposure, fibroblasts sense the light-activated cell adhesive ligand and migrate out of the spheroid. C) 3D culture of optogenetically-engineered bacteria able to produce a certain protein (RFP) or drug (dVio) upon light exposure by activation of an optogenetic switch.

implanted cells or biomaterials opens application possibilities for this approach in a clinical context, that is, cell therapies and optogenetic-based therapies.

### 2.7.2. Application of Printed Waveguides to Remotely Control Drug Release from an Optogenetically-Engineered Living Material

To demonstrate that the printed waveguides can be used to trigger optogenetic processes in cells, we stimulated bacteria that were genetically engineered to produce a protein or a drug upon activation of an optogenetic switch. For this purpose, the pDawn<sup>[38]</sup> plasmid for optogenetic protein expression, and the red fluorescent protein (RFP)<sup>[35b]</sup> or the *vioABCE* operon,<sup>[35a]</sup> were cloned into a commercially available endotoxin-free *E. coli* strain (ClearColi).<sup>[39]</sup> Upon exposure to blue light, the encapsulated bacteria start expression of RFP or the enzymes *vioA*, *vioB*, *vioC*, and *vioE* that catalyze the production of deoxyviolacein (dVio), a therapeutic drug. The bacteria were encapsulated in a polymeric matrix to form a living therapeutic construct for controlled drug delivery.<sup>[35]</sup> In order to quantify the amount of released

drug as a function of light exposure, the bacteria-containing hydrogel was placed in a transwell insert which allows the release of the drug to the surrounding medium.<sup>[35a,40]</sup> The hydrogel containing the optogenetically-engineered bacteria was exposed with blue light (450 nm) delivered by a printed PEGDA-DTT-50 (70 wt%) waveguide after passing through 8 cm of porcine tissue. At the distal end of the fiber, the intensity of blue light was around 160 mW cm<sup>-2</sup> (Table S1, Supporting Information) and the illuminated area of hydrogel was in the range of 0.5–1 cm<sup>2</sup>, which covered the entire well containing the bacteria-laden hydrogel. All bacteria could therefore be activated by the out-coupled blue light. For the photoactivated expression of RFP, the irradiation was maintained for 3.5 h, after which epifluorescence microscopy was used to image and quantify the fluorescence intensity (Figure 6A,B). The irradiated bacterial hydrogel developed threefold higher fluorescence intensity than the non-irradiated control, courtesy of activation of bacterial RFP production by blue light delivered by the printed optical waveguide. The fluorescence generated in the non-irradiated hydrogel occurs due to leaky expression of proteins in the absence of light, which is an inherent limitation of

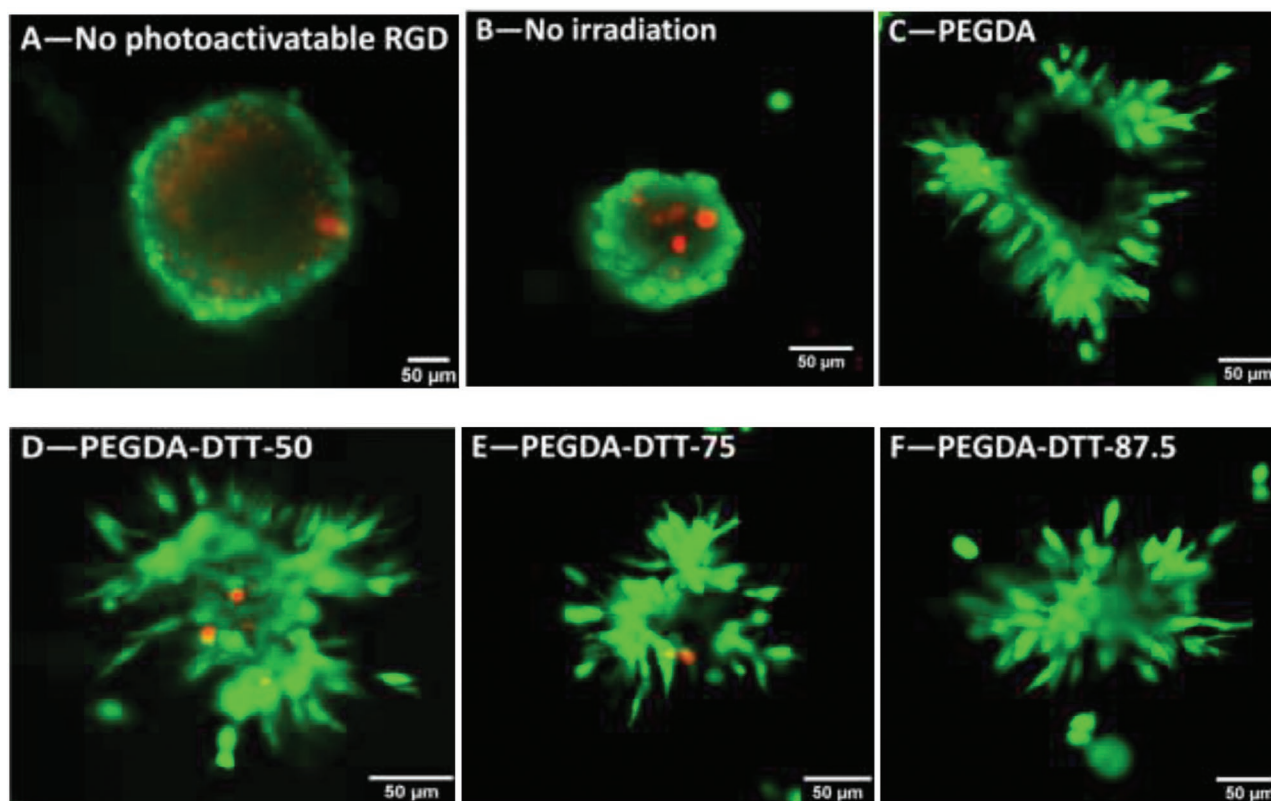


**Figure 5.** Confocal microscopy images of L929 spheroids encapsulated in dextran hydrogels: A) Spheroid in hydrogel that was not functionalized with cyclo[RGD(DMNPB)fC] and was irradiated for 15 min by light (405 nm) guided in PEGDA waveguide through 5 cm tissue; B) spheroid in a hydrogel that was functionalized with cyclo[RGD(DMNPB)fC] but not irradiated by light; C–F) spheroids in hydrogels that were functionalized with cyclo[RGD(DMNPB)fC] and irradiated by light (405 nm) guided in 70 wt% PEGDA (C), PEGDA-DTT-50 (D), PEGDA-DTT-75 (E), and PEGDA-DTT-87.5 (F) waveguides through 5 cm tissue.

optogenetic gene expression systems.<sup>[35a,38,41]</sup> These results demonstrate that the printed waveguides are suitable for activation of optogenetic processes deep inside tissues. The experiment with dVio-producing cells further confirmed this statement. The dVio-producing bacterial hydrogel was irradiated for 4 h followed by culturing at 30 °C protected from light for 1 day to allow the production and secretion of drug. The exposed gel released a significantly higher amount of drug than the non-irradiated control (Figure 6C) as a result of the activation of bacteria by the blue light delivered by the optical waveguide. These results provide an additional demonstration of the capability of the printed waveguides to guide blue light deep into tissue.

## 2.8. Core-Cladding Optical Waveguides

Core-cladding designs in optical waveguides improve the light guiding efficiency by enhancing total internal reflection. To test whether core-cladding designs could improve the waveguiding properties of PEGDA-DTT waveguides, a coaxial printing process with Pluronic F127 was developed. Pluronic F127 is a polymer approved by the U.S. Food and Drug Administration for pharmaceutical applications,<sup>[42]</sup> and forms thermoreversible

gels in aqueous solution.<sup>[43]</sup> By introducing terminal acrylate groups into the Pluronic F127 chains, covalently crosslinked hydrogels can also be obtained by photopolymerization. The RI of 33 wt% Pluronic hydrogel is lower than that of 80 wt% PEGDA-DTT-875 hydrogel (Figure S8A, Supporting Information). These properties make Pluronic F127 a convenient complement to PEGDA-DTT-875 in a core-cladding optical waveguide design.

80 wt% PEGDA-DTT-875 was coextruded with 33 wt% acrylated Pluronic F127 (Pluronic-DA) as cladding material (Figure 7A). Core-cladding fibers with core diameters ranging from 340 to 640 μm and fixed outside diameter (1.02 mm) were successfully printed using a coaxial printing needle (Figure 3A: right) by varying the printing pressure of the core and the cladding material (Figure S8C,D, Supporting Information). At room temperature, 33 wt% of Pluronic-DA behaves like a paste that exhibits shear-thinning, which allows it to be easily extruded and provide a support for the liquid PEGDA-DTT-875 solution during the printing of the core-cladding structure. The extruded core and cladding can be simultaneously photocrosslinked through the silicone tube attached to the tip of the coaxial needle, which fixes the core/cladding structure. From the printed core/cladding fibers, a smooth interface between core and cladding was observed (Figure 7A). We assume that

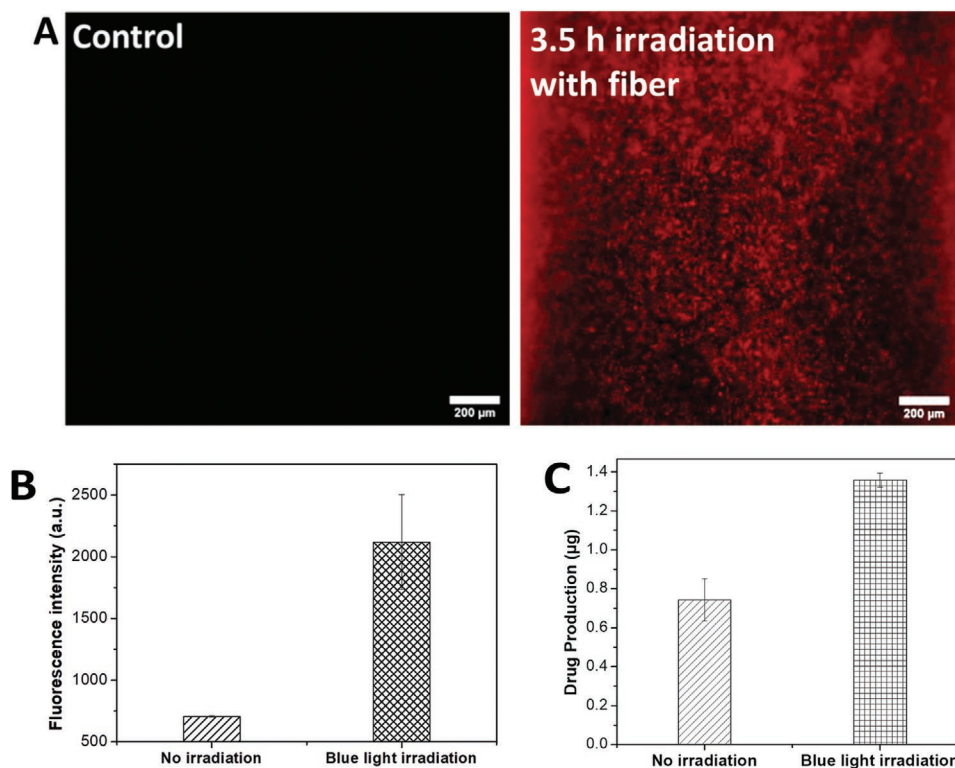


**Figure 6.** A) Fluorescence images of optogenetically-engineered *E. coli* entrapped in 2 wt% agarose hydrogels. Bacteria are programmed to produce RFP upon light exposure. Image on the left shows the bacteria population after 3.5 h in the dark. Image on the right shows the bacteria culture after irradiation for 3.5 h using a PEGDA-DTT-50 waveguide across 8 cm tissue. The secreted RFP makes bacteria become visible under the microscope; B) fluorescence intensity of the bacteria-containing hydrogel with or without exposure to 450 nm light as measured at the surface of the hydrogel. C) Concentration of dVio drug released from optogenetically-engineered bacteria 1 day after irradiation at 450 nm for 3 h using a PEGDA-DTT-50 waveguide across 8 cm tissue. The control was not illuminated.

the two materials are covalently bound to each other by cross-polymerization of the acrylate groups present at the interface of the core and cladding.

The light guiding properties of core-cladding waveguides with 80 wt% PEGDA-DTT-87.5 core and 33 wt% Pluronic-DA cladding were explored and compared with the single PEGDA-DTT-87.5 (65 wt%, to give the same overall water content as in the core/cladding fibers) waveguide design. Core-cladding waveguides with optical loss of  $<0.2 \text{ dB cm}^{-1}$  at 405 nm in air were obtained (Figure 7B), significantly better than the optical loss of single fibers (around  $0.4 \text{ dB cm}^{-1}$ ). This corresponds to longer propagation distances both in air and in tissue (Figure 7C and Figure S8B, Supporting Information). The improved light guiding properties can be attributed to i) the consistent RI difference between core and cladding (Figure S8A, Supporting Information) aiding total internal reflection to better confine light propagation to the core, and ii) the presence of cladding ensuring a consistently smooth interface between the core and its surrounds (while direct contact between core-only and tissue can introduce roughness that increases scattering). Finally, core-cladding waveguides were also tested in their ability to remotely trigger cell migration within a photoactivatable hydrogel after passing through 5 cm muscle tissue. The delivered light by core-cladding fibers successfully activated cell migration (Figure 7D).

### 3. Conclusion

PEGDA-DTT monomers can be easily synthesized from commercially available precursors, and converted to hydrogels by photopolymerization of the terminal acrylate functionalities. These gels are cytocompatible and present adjustable degradability and mechanical properties. The introduction of DTT bridges increases the transparency and decreases light scattering in the hydrogels, mainly as a consequence of higher molar mass and the introduction of free hydroxyl groups with the DTT bridges. The high transparency can be exploited for waveguiding. The hydrogels can be easily printed to produce optical waveguides with optical losses in the visible range of  $0.1\text{--}0.4 \text{ dB cm}^{-1}$  in air and  $0.25\text{--}0.7 \text{ dB cm}^{-1}$  in tissue. This performance rivals the best hydrogel-based waveguides reported to date. Sufficient light can be delivered through many centimeters of porcine tissue to activate optogenetic switches in cells, and control cell adhesion and migration in light-responsive hydrogels. The provided examples demonstrate the practical potential of printed PEGDA-DTT hydrogel waveguides for in vivo control of biological processes and clinical applications. The adjustable degradability allows degradation kinetics to be tailored to the preferred duration of the therapeutic treatment, and the broad range of mechanical properties allows stiffness matching with organs of interest, offering flexibility for customized, light-triggered therapies.

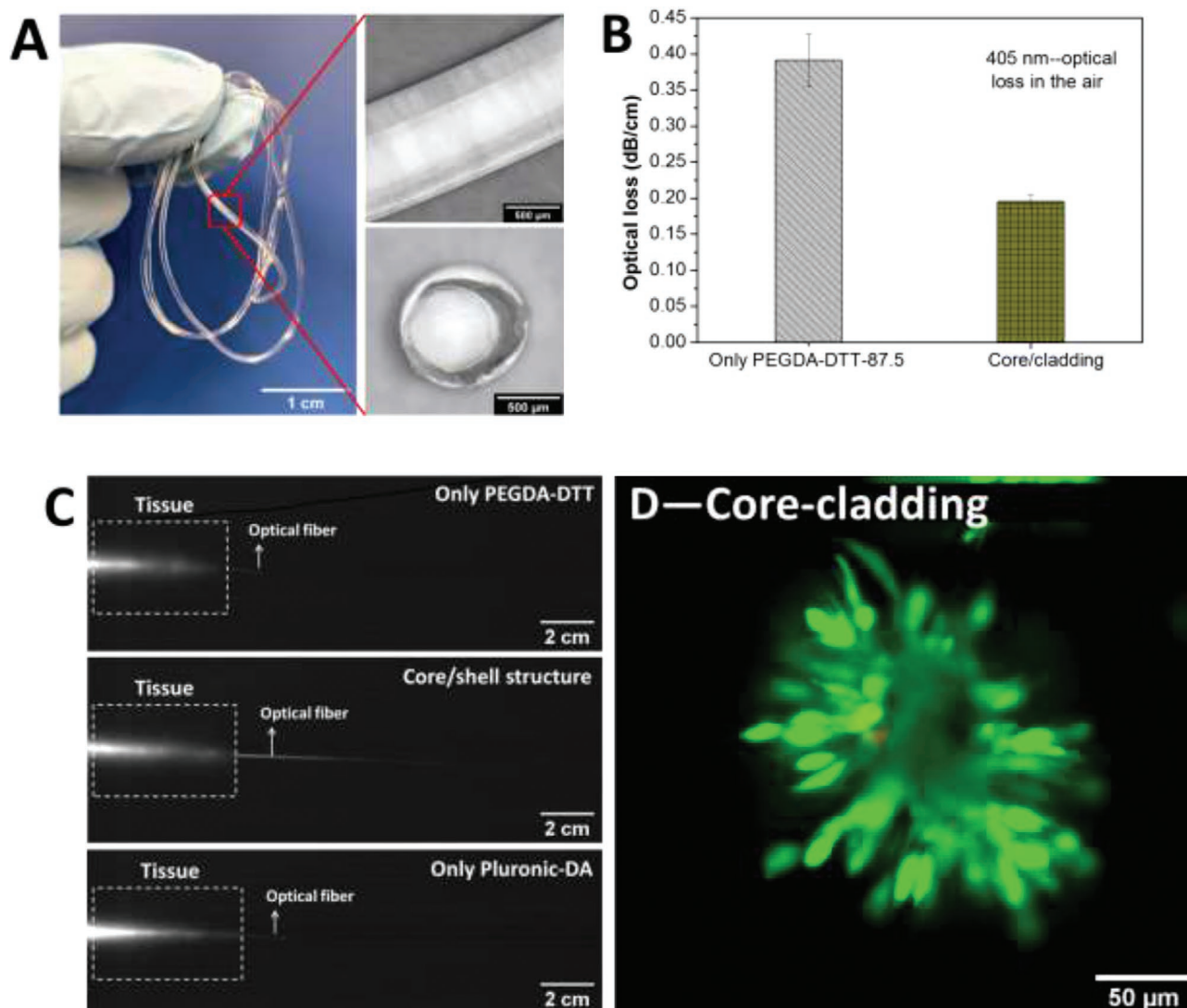


**Figure 7.** A) Images of printed core/cladding fibers (80 wt% of PEGDA-DTT-87.5 for core, 33 wt% of Pluronic-DA for cladding). Left: printed core/cladding fibers, right: magnified images of core/cladding fiber and the cross-section of the fiber. B) Optical loss of single fiber and core/cladding fibers at 405 nm; C) image of 405 nm light beam propagating through core-only and core/cladding waveguides in tissue. D) Spheroids in hydrogels that were functionalized with cyclo[RGD(DMNPB)fC] and irradiated by light (405 nm) guided in core-cladding waveguides (PEGDA-DTT-87.5 as core, Pluronic-DA as cladding) through 5 cm tissue.

## Supporting Information

Supporting Information is available from the Wiley Online Library or from the author.

## Acknowledgements

Authors thank Dr. Peter Rogin for the help with building home-made setups for light guiding and scattering measurements, and thank Qiyang Jiang for providing caged RGD. J.F. thanks Dr. Malgorzata Katarzyna Wlodarczyk-Biegun for training on the printing equipment. pDawn was a gift from Andreas Möglich (Addgene plasmid # 43796). J.F. acknowledges the funding from China Scholarship Council (CSC) grant 201506950062.

Open access funding enabled and organized by Projekt DEAL.

## Conflict of Interest

The authors declare no conflict of interest.

## Keywords

3D printing, biophotonics, degradable waveguides, optical waveguides, optogenetics

Received: May 19, 2020

Revised: July 15, 2020

Published online: September 2, 2020

- [1] a) V. V. Tuchin, *Handbook of Photonics for Biomedical Science*, CRC Press, Boca Raton, FL **2010**; b) A. Méndez, in *Optics in Our Time* (Eds: M. D. Al-Amri, M. El-Gomati, M. S. Zubairy), Springer, Cham **2016**, p. 299; c) F. Zhang, A. M. Aravanis, A. Adamantidis, L. de Lecea, K. Deisseroth, *Nat. Rev. Neurosci.* **2007**, *8*, 577; d) S. H. Yun, S. J. Kwok, *Nat. Biomed. Eng.* **2017**, *1*, 0008; e) J. C. Williams, T. Denison, *Sci. Transl. Med.* **2013**, *5*, 177ps6; f) K. Deisseroth, *Nat. Methods* **2011**, *8*, 26; g) O. Yizhar, L. E. Fenno,

- T. J. Davidson, M. Mogri, K. Deisseroth, *Neuron* **2011**, *71*, 9; h) L. Fenno, O. Yizhar, K. Deisseroth, *Annu. Rev. Neurosci.* **2011**, *34*, 389; i) E. Pastrana, *Nat. Methods* **2010**, *8*, 24.
- [2] L. Beauté, N. McClenaghan, S. Lecommandoux, *Adv. Drug Delivery Rev.* **2018**, *138*, 148.
- [3] a) G. Mayer, A. Heckel, *Angew. Chem., Int. Ed.* **2006**, *45*, 4900; b) N. Ankenbruck, T. Courtney, Y. Naro, A. Deiters, *Angew. Chem., Int. Ed.* **2018**, *57*, 2768; c) T. Courtney, A. Deiters, *Curr. Opin. Chem. Biol.* **2018**, *46*, 99.
- [4] S. Nizamoglu, M. C. Gather, M. Humar, M. Choi, S. Kim, K. S. Kim, S. K. Hahn, G. Scarcelli, M. Randolph, R. W. Redmond, *Nat. Commun.* **2016**, *7*, 10374.
- [5] a) C. M. Lee, C. J. Engelbrecht, T. D. Soper, F. Helmchen, E. J. Seibel, *J. Biophotonics* **2010**, *3*, 385; b) P. Kim, E. Chung, H. Yamashita, K. E. Hung, A. Mizoguchi, R. Kucherlapati, D. Fukumura, R. K. Jain, S. H. Yun, *Nat. Methods* **2010**, *7*, 303; c) R. Kiesslich, M. Goetz, E. M. Angus, Q. Hu, Y. Guan, C. Potten, T. Allen, M. F. Neurath, N. F. Shroyer, M. H. Montrose, *Gastroenterology* **2007**, *133*, 1769.
- [6] S. Shabahang, S. Kim, S. H. Yun, *Adv. Funct. Mater.* **2018**, *28*, 1706635.
- [7] R. Fu, W. Luo, R. Nazempour, D. Tan, H. Ding, K. Zhang, L. Yin, J. Guan, X. Sheng, *Adv. Opt. Mater.* **2018**, *6*, 1700941.
- [8] a) S. T. Parker, P. Domachuk, J. Amsden, J. Bressner, J. A. Lewis, D. L. Kaplan, F. G. Omenetto, *Adv. Mater.* **2009**, *21*, 2411; b) M. B. Applegate, G. Perotto, D. L. Kaplan, F. G. Omenetto, *Biomed. Opt. Express* **2015**, *6*, 4221; c) S. Kujala, A. Mannilla, L. Karvonen, K. Kieu, Z. Sun, *Sci. Rep.* **2016**, *6*, 22358.
- [9] a) N. Huby, V. Vié, A. Renault, S. Beauvils, T. Lefèvre, F. Paquet-Mercier, M. Pézolet, B. Bèche, *Appl. Phys. Lett.* **2013**, *102*, 123702; b) K. H. Tow, D. M. Chow, F. Vollrath, I. Dicaire, T. Gheysens, L. Thévenaz, *J. Lightwave Technol.* **2017**, *36*, 1138;
- [10] A. Dupuis, N. Guo, Y. Gao, N. Godbout, S. Lacroix, C. Dubois, M. Skorobogatiy, *Opt. Lett.* **2007**, *32*, 109.
- [11] A. Jain, A. H. Yang, D. Erickson, *Opt. Lett.* **2012**, *37*, 1472.
- [12] A. K. Manocchi, P. Domachuk, F. G. Omenetto, H. Yi, *Biotechnol. Bioeng.* **2009**, *103*, 725.
- [13] D. Shan, E. Gerhard, C. Zhang, J. W. Tierney, D. Xie, Z. Liu, J. Yang, *Bioact. Mater.* **2018**, *3*, 434.
- [14] a) M. Choi, J. W. Choi, S. Kim, S. Nizamoglu, S. K. Hahn, S. H. Yun, *Nat. Photonics* **2013**, *7*, 987; b) A. Francone, T. Kehoe, I. Obieta, V. Saez-Martinez, L. Bilbao, A. Khokhar, N. Gadegaard, C. Simao, N. Kehagias, C. Sotomayor Torres, *Sensors* **2018**, *18*, 3240; c) Y. J. Heo, H. Shibata, T. Okitsu, T. Kawanishi, S. Takeuchi, *Proc. Natl. Acad. Sci. USA* **2011**, *108*, 13399; d) M. Choi, M. Humar, S. Kim, S. H. Yun, *Adv. Mater.* **2015**, *27*, 4081; e) J. Guo, M. Zhou, C. Yang, *Sci. Rep.* **2017**, *7*, 7902; f) J. Guo, H. Huang, M. Zhou, C. Yang, L. Kong, *Anal. Chem.* **2018**, *90*, 12292; g) A. K. Yetisen, N. Jiang, A. Fallahi, Y. Montelongo, G. U. Ruiz-Esparza, A. Tamayol, Y. S. Zhang, I. Mahmood, S. A. Yang, K. S. Kim, *Adv. Mater.* **2017**, *29*, 1606380; h) N. Jiang, R. Ahmed, A. A. Rifat, J. Guo, Y. Yin, Y. Montelongo, H. Butt, A. K. Yetisen, *Adv. Opt. Mater.* **2018**, *6*, 1701118; i) M. Zhou, J. Guo, C. Yang, *Sens. Actuators, B* **2018**, *264*, 52; j) S. Johannsmeier, M. Torres, T. Ripken, D. Heinemann, A. Heisterkamp, *Proc. SPIE* **2018**, *10482*, 104820Q; k) L. Zhao, J. Gan, T. Xia, L. Jiang, J. Zhang, Y. Cui, G. Qian, Z. Yang, *J. Mater. Chem. C* **2019**, *7*, 897; l) M. Elsharif, R. Moreddu, M. U. Hassan, A. K. Yetisen, H. Butt, *Lab Chip* **2019**, *19*, 2060; m) M. Elsharif, M. U. Hassan, A. K. Yetisen, H. Butt, *Biosens. Bioelectron.* **2019**, *137*, 25.
- [15] a) J. Guo, X. Liu, N. Jiang, A. K. Yetisen, H. Yuk, C. Yang, A. Khademhosseini, X. Zhao, S. H. Yun, *Adv. Mater.* **2016**, *28*, 10244; b) L. Wang, C. Zhong, D. Ke, F. Ye, J. Tu, L. Wang, Y. Lu, *Adv. Opt. Mater.* **2018**, *6*, 1800427.
- [16] a) J. Missinne, S. Kalathimekkad, B. Van Hoe, E. Bosman, J. Vanfleteren, G. Van Steenberge, *Opt. Express* **2014**, *22*, 4168; b) M. Ramuz, B. C. K. Tee, J. B. H. Tok, Z. Bao, *Adv. Mater.* **2012**, *24*, 3223; c) C. To, T. L. Hellebrekers, Y.-L. Park, in *IEEE/RSJ Int. Conf. on Intelligent Robots and Systems (IROS)*, IEEE, Piscataway, NJ **2015**, pp. 5898–5903; d) S. J. Kwok, M. Kim, H. H. Lin, T. G. Seiler, E. Beck, P. Shao, I. E. Kochevar, T. Seiler, S.-H. Yun, *Invest. Ophthalmol. Visual Sci.* **2017**, *58*, 2596; e) S. J. Kwok, S. Forward, C. M. Wertheimer, A. C. Liapis, H. H. Lin, M. Kim, T. G. Seiler, R. Birngruber, I. E. Kochevar, T. Seiler, *Investigative Ophthalmol. Visual Sci.* **2019**, *60*, 2563; f) J. Guo, M. Niu, C. Yang, *Optica* **2017**, *4*, 1285; g) J. Guo, B. Zhou, C. Yang, Q. Dai, L. Kong, *Adv. Funct. Mater.* **2019**, *29*, 1902898; h) M. Kolle, A. Lethbridge, M. Kreysing, J. J. Baumberg, J. Aizenberg, P. Vukusic, *Adv. Mater.* **2013**, *25*, 2239; i) I. Martincek, D. Pudis, P. Gaso, *IEEE Photonics Technol. Lett.* **2013**, *25*, 2066; j) J. Missinne, G. Van Steenberge, B. Van Hoe, K. Van Coillie, T. Van Gijsegem, P. Dubruel, J. Vanfleteren, P. Van Daele, *Proc. SPIE* **2009**, *7221*, 722105.
- [17] a) M. Kim, J. An, K. S. Kim, M. Choi, M. Humar, S. J. Kwok, T. Dai, S. H. Yun, *Biomed. Opt. Express* **2016**, *7*, 4220; b) A. Gierej, M. Vagenende, A. Filipkowski, B. Siwicki, R. Buczynski, H. Thienpont, S. Van Vlierberghe, T. Geernaert, P. Dubruel, F. Berghmans, *J. Lightwave Technol.* **2019**, *37*, 1916.
- [18] W. J. Choi, K. S. Park, B. H. Lee, *J. Biomed. Opt.* **2014**, *19*, 090503.
- [19] S. Shabahang, S. Forward, S.-H. Yun, *Opt. Express* **2019**, *27*, 7560.
- [20] D. Shan, C. Zhang, S. Kalaba, N. Mehta, G. B. Kim, Z. Liu, J. Yang, *Biomaterials* **2017**, *143*, 142.
- [21] a) M. S. Wartak, *Computational Photonics: An Introduction with MATLAB*, Cambridge University Press, Cambridge **2013**; b) J. Turkiewicz, *2018 20th Int. Conf. on Transparent Optical Networks (ICTON)*, IEEE, Piscataway, NJ **2018**, pp. 1–4.
- [22] H. Ma, A. Y. Jen, L. R. Dalton, *Adv. Mater.* **2002**, *14*, 1339.
- [23] L. Ouyang, C. B. Highley, W. Sun, J. A. Burdick, *Adv. Mater.* **2017**, *29*, 1604983.
- [24] G. A. Hudalla, T. S. Eng, W. L. Murphy, *Biomacromolecules* **2008**, *9*, 842.
- [25] a) Q. T. Nguyen, Y. Hwang, A. C. Chen, S. Varghese, R. L. Sah, *Biomaterials* **2012**, *33*, 6682; b) S. M. LaNasa, I. T. Hoffecker, S. J. Bryant, *J. Biomed. Mater. Res., Part B* **2011**, *96*, 294.
- [26] P. Van de Wetering, A. T. Metters, R. G. Schoenmakers, J. A. Hubbell, *J. Controlled Release* **2005**, *102*, 619.
- [27] S. L. Jacques, *Phys. Med. Biol.* **2013**, *58*, R37.
- [28] a) A. Mehta, *Pharma XChange* **2011**, *13*, 12; b) D. A. Skoog, F. J. Holler, S. R. Crouch, *Principles of Instrumental Analysis*, Cengage Learning, Boston, MA **2017**.
- [29] a) D. O'Carroll, I. Lieberwirth, G. Redmond, *Small* **2007**, *3*, 1178; b) F. Gu, H. Yu, P. Wang, Z. Yang, L. Tong, *ACS Nano* **2010**, *4*, 5332; c) D. Di Camillo, V. Fasano, F. Ruggieri, S. Santucci, L. Lozzi, A. Camposeo, D. Pisignano, *Nanoscale* **2013**, *5*, 11637.
- [30] H.-X. Xu, Y. Tan, D. Wang, X.-L. Wang, W.-L. An, P.-P. Xu, S. Xu, Y.-Z. Wang, *Soft Matter* **2019**, *15*, 3588.
- [31] D. Grant, J. Miller, D. T. Burns, *J. Chromatogr., A* **1973**, *79*, 267.
- [32] X. Ma, X. Sun, D. Hargrove, J. Chen, D. Song, Q. Dong, X. Lu, T.-H. Fan, Y. Fu, Y. Lei, *Sci. Rep.* **2016**, *6*, 19370.
- [33] a) R. Ramaswami, K. Sivarajan, G. Sasaki, *Optical Networks: A Practical Perspective*, Morgan Kaufmann, Burlington, MA **2009**; b) B. G. Potter, *Module 3 - Attenuation in Optical Fibers*, Material Science and Engineering Dept., University of Arizona **2010**, 1.
- [34] a) Y. Zheng, M. K. L. Han, Q. Jiang, B. Li, J. Feng, A. del Campo, *Mater. Horiz.* **2019**, *7*, 111; b) A. Farrukh, J. I. Paez, A. del Campo, *Adv. Funct. Mater.* **2019**, *29*, 1807734.
- [35] a) S. Sankaran, J. Becker, C. Wittmann, A. del Campo, *Small* **2019**, *15*, 1804717; b) S. Sankaran, A. del Campo, *Adv. Biosyst.* **2019**, *3*, 1800312.
- [36] a) M. J. Salierno, A. J. García, A. del Campo, *Adv. Funct. Mater.* **2013**, *23*, 5974; b) S. Petersen, J. M. Alonso, A. Specht, P. Duodu, M. Goeldner, A. del Campo, *Angew. Chem., Int. Ed.* **2008**, *47*, 3192;

- c) Y. Ohmuro-Matsuyama, Y. Tatsu, *Angew. Chem., Int. Ed.* **2008**, *47*, 7527; d) M. Wirkner, J. M. Alonso, V. Maus, M. Salierno, T. T. Lee, A. J. García, A. del Campo, *Adv. Mater.* **2011**, *23*, 3907; e) M. Wirkner, S. Weis, V. San Miguel, M. Álvarez, R. A. Gropeanu, M. Salierno, A. Sartoris, R. E. Unger, C. J. Kirkpatrick, A. del Campo, *ChemBioChem* **2011**, *12*, 2623.
- [37] T. T. Lee, J. R. García, J. I. Paez, A. Singh, E. A. Phelps, S. Weis, Z. Shafiq, A. Shekaran, A. Del Campo, A. J. García, *Nat. Mater.* **2015**, *14*, 352.
- [38] R. Ohlendorf, R. R. Vidavski, A. Eldar, K. Moffat, A. Möglich, *J. Mol. Biol.* **2012**, *416*, 534.
- [39] U. Mamat, K. Wilke, D. Bramhill, A. B. Schromm, B. Lindner, T. A. Kohl, J. L. Corchero, A. Villaverde, L. Schaffer, S. R. Head, *Microb. Cell Fact.* **2015**, *14*, 57.
- [40] N. Grossman, E. Z. Ron, C. L. Woldringh, *J. Bacteriol.* **1982**, *152*, 35.
- [41] a) J. Fernandez-Rodriguez, F. Moser, M. Song, C. A. Voigt, *Nat. Chem. Biol.* **2017**, *13*, 706; b) A. Baumschlager, S. K. Aoki, M. Khammash, *ACS Synth. Biol.* **2017**, *6*, 2157.
- [42] G. Dumortier, J. L. Grossiord, F. Agnely, J. C. Chaumeil, *Pharm. Res.* **2006**, *23*, 2709.
- [43] G. Dumortier, J. Grossiord, M. Zuber, G. Couarraze, J. Chaumeil, *Drug Dev. Ind. Pharm.* **1991**, *17*, 1255.